Exploring linear plasma response for RMP ELM mitigation and suppression in MAST-U

E. Tomasina[1,2], L.Pigatto[2], D.Ryan[4], Y.Q. Liu[5] , C.Albert[3], M.Markl[3], E.Viezzer[6], T. Bolzonella[2], MAST-U team[4] and the EUROfusion Tokamak Exploitation Team*

[1]*Università degli Studi di Padova, Padova, Italy.* [2] *Consorzio RFX (CNR, ENEA, INFN, Università di Padova, Acciaierie Venete SpA), Corso Stati Uniti 4 – 35127 – Padova (Italy)* [3] *Fusion@OEAW, Graz University of Technology, Graz, Austria.* [4] *3UKAEA, Culham Campus, Abingdon OX14 3DB, UK.* [5] *General Atomics, PO Box 85608, San Diego, CA 92186-5608, USA.* [6] *Department of Atomic, Molecular and Nuclear Physics, University of Seville, Seville, Spain.*

Introduction

Edge Localized Modes (ELMs) are pressure-current hybrid MHD instabilities which periodically lead to violent expulsion of heat and particles in a filament fashion [1]. Controlling (i.e., either pacing, mitigating, or suppressing) ELMs is of crucial importance for the safety of future fusion reactors. While ELMs control via Resonant Magnetic Perturbations (RMPs) was achieved in the previous iteration of the MAST experiment [2], it is currently proving challenging to replicate this success in the MAST-U device. Recent campaigns have shown mixed results: either enough effectiveness to trigger mode-locking and subsequent disruptions or no significant effect at all [3]. Key differences between MAST-U and its predecessor include the structure of the non-axisymmetric coil system[4]. In MAST-U, the system has been reduced in both the maximum current amplitude and the number of independently supplied coils. This, in turn, reduces the achievable toroidal spectrum compared to MAST. However, the plasma size has been increased, bringing the boundary closer to the coils[3]. As a result, similar order of magnitudes of field perturbations can still be generated. Additionally, having recently started operations, MAST-U scenarios have not been fully developed. Only Connected Double Null (CDN) discharges have been achieved so far, with no Single Null (SN) plasmas developed yet. It is known that achieving ELM control is more challenging in CDN discharges due to the reduced plasma response developed at the High Field Side (HFS) [5]. Finally, recent experimental results and comparisons with modeling have raised suspicions of a residual Error Field (EF) dominated by an n=2 component[3]. This may explain why the modeling has so far failed to predict the optimal phase for achieving mitigation and will be a focus of future investigations.

Modeling ELMs control in tight geometry

Understanding the plasma response is crucial for tailoring magnetic perturbations to mitigate or suppress ELMs. While the full mechanism controlling ELMs remains incompletely understood, valuable insights have emerged from comparing experimental data with modeling outcomes. Current literature highlights several metrics that correlate with ELM control, often computable using linearized models, allowing for rapid optimization of external coil parameters[6].

*See the author list of "Overview of the EUROfusion Tokamak Exploitation programme in support of ITER and DEMO" by E. Joffrin Nuclear Fusion 2024 10.1088/1741-4326/ad2be4

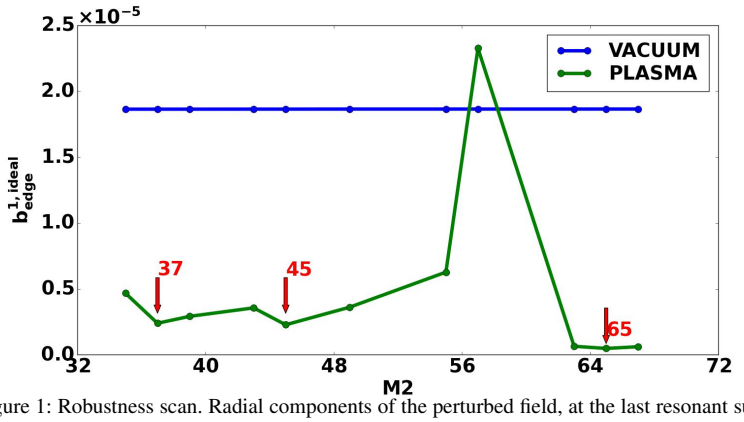

Figure 1: Robustness scan. Radial components of the perturbed field, at the last resonant surface, in the ideal approximation vs number of positive harmonics for the poloidal angle decomposition. *Blue* shows the vacuum field only, whereas *Green* considers also the plasma response. *Red arrows* indicate the position of local minima of the curve

In this work, we performed the modeling of the plasma response to n=1 and n=2 external perturbations starting from the #47051 discharge. This shot belongs to the MU-02 campaign, during which experiments for ELM control were performed by injecting n=2 RMP, but no overall effect was observed. Input data were collected at $\sim$ 500 ms. The plasma equilibrium has been reconstructed with magnetic measurements and constrained with the MSE measurement. Moreover, temperatures, density, and rotational flow profiles were made available by MAST-U diagnostics and mapped on the EFIT equilibrium. The calculations have been performed with the CHEASE/MARS-F workflow, which, starting from the equilibrium data, allows for the computation of the field perturbation structure induced via external coils. CHEASE [7] is a fixed-boundary equilibrium code that is routinely implemented to prepare MARS-F inputs. MARS-F [8], in turn, is a 2D-resistive, linear MHD code that implements toroidal geometry and allows the computation of both the vacuum field perturbation injected by a set of external non-axisymmetric coils and the plasma response to it. Exploiting the linearity of the model, i.e., the superposition of MARS-F solutions are still solutions, it holds: $I_{tot} = I_U + I_L e^{i\Delta\Phi}$. With $\Delta\Phi$ being the relative toroidal phase variation. This facilitates rapid quantification of how the perturbation effectiveness varies with the relative phase adjustment between the upper and lower coil sets. In other words, this aims to produce different poloidal spectra to identify the optimal configuration favoring ELM control. The figures of merit chosen for this work are the magnitude of the radial component of the pitch-aligned edge perturbation field b^1_{edge}, the ratio between the plasma displacement at the X points and at midplane, namely ξ_X/ξ_M and the ratio between the torque induced in the edge and in the core region: τ_{edge}/τ_{core}. The first metric is used to quantify how much perturbed field the system can inject in the plasma, whereas the other two keep track of the effects on the confinement[9][10]. MARS-F naturally incorporates toroidal geometry by operating in flux coordinates, it also employs Fourier decomposition to resolve the poloidal angle. This approach makes the number of Fourier coefficients a significant grid parameter for accurately resolving the MHD problem. Since MARS-F cannot fully handle the X-point geometry, the usual procedure involves smoothing the plasma boundary in these regions. This smoothing reduces the number of poloidal harmonics needed for resolution and lowers the edge value of the safety factor q_a; consequently, the number of resonant surfaces within the plasma, for a fixed toroidal number, is reduced as well. As a spheri-

cal tokamak, MAST-U features a tight aspect ratio poloidal section, requiring additional numerical efforts (i.e., more harmonics) to achieve good resolution and ensure decoupling of all resonant surfaces in the plasma. This decoupling is essential to avoid spurious and non-physical contributions. We have observed that after reaching a certain minimum number, which depends on the amount of resonant surfaces inside the plasma (i.e.., on the q_a value), increasing the number of harmonics does not monotonically improve the result's robustness. Figure 1 illustrates this concept using the perturbed field computed in ideal approximation $b^1_{ideal,edge}$ (with one row of coils only) as a probe for robustness. In ideal MHD, currents are expected to build up on rational surfaces in response to perturbations, providing shielding from external fields. Thus, any non-zero $b^1_{ideal,edge}$ value indicates spurious coupling linked to the truncation of the convolution integral. Therefore, the local minima in the robustness scan represent the optimal number of harmonics for performing computations. The results of the modeling for the 47051 discharge are summarized in Table 1 for both cases with n=1 and n=2. To optimize result robustness and computational efficiency, a smoothed equilibrium was taken as input, along with 37 positive harmonics for the poloidal decomposition. A sinusoidal current was induced in the external coil geometry with a unit reference of $I_0 = 1kAt$ to generate the perturbation. For each case, two simulations were performed by activating one row of coils at a time. Additionally, extra MARS-F runs were performed to compute the so-called 'torque matrix', which allows the linearization of the induced torque density (which otherwise would be a quadratic effect). According to the tabulated results, the configurations that maximize the field almost rigidly shift of 70°-80° when going from the n=1 to the n=2 case. Following the same pattern, the maximization of the displacement at the X-points over the midplane's varies of a similar amount. The phase that maximizes the ratio of the total integrated torque in the edge region over the core one, instead, seems to be strongly robust to the variation of the toroidal number of the perturbation, where it is pointed out that the separation between edge and core regions is assumed to lie around 89% of the poloidal flux (see appendix in [10]).

Separatrix density scan

Future operations oversee the installation of a cryopump in the lower divertor to improve density control and allow for detachment [11]. We tried to evaluate the impact of the cryopump installation in terms of coil optimisation for ELMs control by performing a scan in the separatrix density. This

	$b^1_{edge,Vacuum}$	$b^1_{edge,Total}$	ξ_X/ξ_M	τ_{edge}/τ_{core}
n=1	113°	178°	73°, 68°	180°
n=2	193°	247°	156°, 156°	180°

Table 1: optimal ΔΦ for n=1,2 cases according to different metrics. In column 1, only the vacuum perturbation is considered, whereas the results relative to the total field, accounting for plasma response, is displayed in column 2 . In column 3, *blue* highlights the optimization with respect to the upper X-point, while *red* refers to the lower X-point. Finally, in column 4, we report the optimization with respect to the induced torque ratio between edge and core regions.

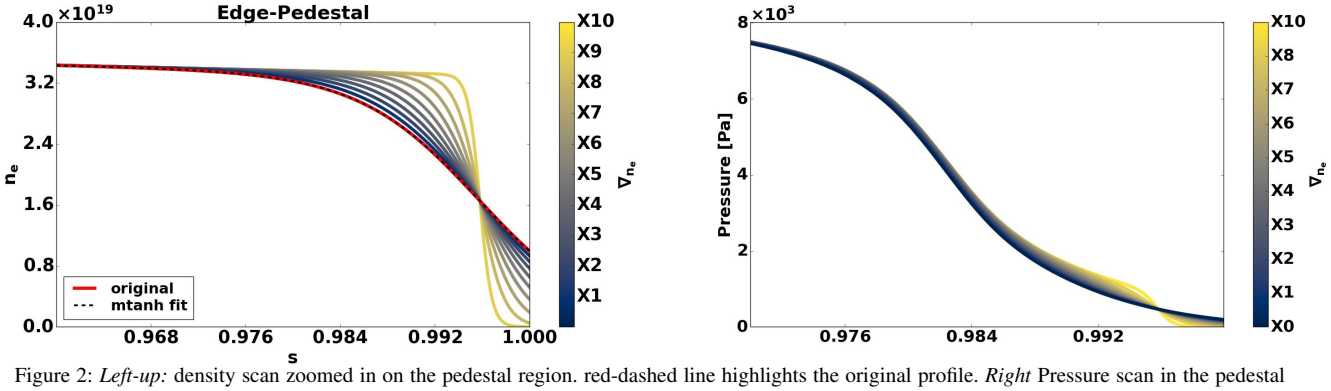

Figure 2: *Left-up:* density scan zoomed in on the pedestal region. red-dashed line highlights the original profile. *Right* Pressure scan in the pedestal region.

formally corresponds to a scan in the pedestal width while keeping fixed the pedestal top height. In this work, we focused on the n=2 case and increased the pedestal gradient by up to a factor of 10, resulting in a decrease of $n_{e,sep}$ by approximately 100-fold. Assuming no extra input power would be inserted in the plasma, the ionic and electronic temperatures have been left invariant. As a consequence, the scan is not isobaric, and we had to re-calculate the equilibrium by providing recomputed pressure profiles considering only the thermal contribution: $P_{new} = n_e \cdot k_B(T_e + T_i)$, for each n_e profile of the scan. In Table 2 we report the main results of the pedestal gradient scan in terms of the b^1_{edge} and ξ_x/ξ_M metrics. In general, the optimal $\Delta\phi$ tends to decrease as the density gradient increases when considering the radial field magnitude metrics. Conversely, the displacement ratio metric shows an increase in optimal $\Delta\phi$ with a rising density gradient. In both cases, the last two or three points of the scan diverge from the general trend, possibly indicating a different type of response. In conclusion, note that the term 'X1' in the column refers to the same density profile as in the original case. Therefore, any discrepancies with the results reported in Table 1 should be attributed to the difference between the equilibria recomputed with the thermal pressure and the original one. The significant variation in the optimal value of $\xi_{X,L}/\xi_M$, for example, stresses the importance of including kinetic constraints when calculating equilibrium solutions.

∇n_e	X1	X2	X3	X4	X5	X6	X7	X8	X9	X10
$b^1_{edge,Tot}$	236°	236°	233°	229°	222°	218°	207°	204°	207°	236°
$\xi_{X,U}/\xi_M$	151°	155°	160°	170°	185°	199°	218°	238°	233°	238
$\xi_{X,L}/\xi_M$	214°	219°	224°	238°	253°	287°	340°	24°	29°	340°

Table 2: optimal ΔΦ for n=2 case, scanning the density pedestal gradient according to the maximum field and maximum displacement ratio metrics

References

[1] Hartmut Zohm. In: *Control. Fusion* 38 (1996), pp. 1213–1223.
[2] A. Kirk et al. In: *Nuclear Fusion* 50 (3 2010). ISSN: 00295515. DOI: 10.1088/0029-5515/50/3/034008.
[3] D A Ryan et al. In: *Submitted to Plasma Physics and Controlled Fusion* (2024).
[4] L. Piron et al. In: *Fusion Engineering and Design* (Dec. 2020). DOI: 10.1016/j.fusengdes.2020.111932.
[5] M W Shafer et al. In: *28th IAEA Fusion Energy Conference (FEC), London* (2020).
[6] Yueqiang Liu et al. In: *Plasma Phys. Control. Fusion* (2016).
[7] H Ltitjens, A Bondeson, and O Sauter. In: *Computer Physics Communications* 97 (1996), pp. 219–260.
[8] Y. Q. Liu et al. In: *Physics of Plasmas* 7 (9 2000), pp. 3681–3690. ISSN: 1070664X. DOI: 10.1063/1.1287744.
[9] L Pigatto et al. In: *Nucl. Fusion 6* (2023).
[10] L. Li et al. In: *Nuclear Fusion* 59 (9 Aug. 2019). ISSN: 17414326. DOI: 10.1088/1741-4326/ab2bca.
[11] Joe Milnes et al. In: *Fusion Engineering and Design* 96-97 (2015). DOI: 10.1016/j.fusengdes.2015.03.002.